# Adiabatic Air Dehumidification in Laminar Flow Desiccant Matrices

Ahmad A. Pesaran

July 1987

## NOTICE

# ADIABATIC AIR DEHUMIDIFICATION IN LAMINAR FLOW DESICCANT MATRICES

A. A. Pesaran
Solar Energy Research Institute
Golden, Colorado 80401

## ABSTRACT

Adiabatic step transient heat- and mass-transfer and pressure drop experimental data were obtained for a dehumidifier test matrix that contained microbead-silica-gel desiccant in a parallel-plate geometry. The data were analyzed and compared with the results of two other test dehumidifiers: a parallel-plate matrix using crushed silica gel, and a staggered, parallel-strip matrix using microbead silica gel. The analysis showed that the overall heat- and mass-transfer Nusselt numbers of the staggered, parallel-strip matrix were about 70% to 80% larger than those of the parallel-plate matrices. It also showed that the solid-side resistance to moisture diffusion in the smaller microbead silica gel was about 45% less than that of crushed silica gel because the particle size was 60% smaller. The ratio of heat- or mass-transfer coefficient to pressure drop of the microbead-silica-gel staggered, parallel-strip matrix was higher than the other two test dehumidifiers. Based on these findings, a dehumidifier using microbead silica-gel in a staggered, parallel-strip geometry can be made more compact than the other combinations.

## NOMENCLATURE

| | |
|---|---|
| $a$ | surface area per unit volume (1/m) |
| $A$ | matrix wet surface area of coated tape ($m^2$) |
| $A_c$ | matrix minimum flow area ($m^2$) |
| $d_h$ | heat or mass transfer hydraulic diameter (mm) |
| $d_h'$ | momentum hydraulic diameter (mm) |
| $d_p$ | particle diameter ($\mu m$) |
| $D_w$ | moisture diffusivity in air ($m^2/s$) |
| $D_W$ | moisture diffusivity in solid particles ($m^2/s$) |
| $f$ | Fanning friction factor |
| $f_\infty$ | local Fanning friction factor for fully developed flow |
| $F_i$ | ith combined potential |
| $h_{mg}$ | convective or gas-side mass transfer coefficient ($kg/m^2$ s) |
| $k$ | thermal conductivity of moist air (W/m K) |
| $K$ | pressure-drop coefficient |
| $\ell$ | streamwise length of strips ($\mu m$) |
| $L$ | axial length of the matrix (m) |
| $Le$ | effective Lewis number |
| $m_d$ | active mass of dry desiccant (kg) |
| $m_{des}$ | actual mass of dry desiccant (kg) |
| $\dot{m}_a$ | dry air mass flow rate (kg/s) |
| $Nu$ | convective heat-transfer Nusselt number |
| $Nu_m$ | convective mass-transfer Nusselt number |
| $Nu_{mo}$ | overall mass-transfer Nusselt number |
| $Nu_o$ | overall heat-transfer Nusselt number |
| $N_{tu}$ | number of heat-transfer units |
| $P_f$ | packing factor |
| $P$ | pressure (Pa) |
| $Pr$ | Prandtl number |
| $R_d$ | ratio of effective mass to actual mass of dry desiccant ($m_d/m_{des}$) |
| $Re$ | Reynolds number |
| $s$ | streamwise spacing between strips ($\mu m$) |
| $S_g$ | gas-side mass-transfer resistance ($sm^2/kg$) |
| $S_o$ | overall mass transfer resistance ($sm^2/kg$) |
| $S_s$ | solid-side mass transfer resistance ($sm^2/kg$) |
| $T$ | temperature (K) |
| $T'$ | dimensionless temperature |
| $u$ | air axial velocity in the channels (m/s) |
| $w$ | humidity ratio (kg water/kg dry air) |

1

| W | desiccant water content (kg water/kg dry desiccant) |
|---|---|
| $X_{gap}$ | air gap between sheets (μm) |
| $X_{sh}$ | total sheet thickness including the desiccant (μm) |

Greek

| | |
|---|---|
| α | thermal diffusivity of air (m$^2$/s) |
| $\alpha_i$ | $-(\partial T/\partial W)_{F_i}$ |
| ΔP | pressure drop (Pa) |
| $\eta_a$ | solid-side geometry factor coefficient |
| θ' | dimensionless time |
| θ | time (s) |
| μ | statistical mean, also viscosity (Ns/m$^2$) |
| ρ | density (kg/m$^3$) |
| $\rho_d$ | density of particles (kg/m$^3$) |
| σ | standard deviation |
| $\zeta_c$ | solid-side geometry factor |

Subscripts

| | |
|---|---|
| 1 | related to first combined potential |
| 2 | related to second combined potential |
| i | in |
| m | mean value |
| o | out |
| s | start |
| t | total |
| T | at constant temperature |
| ∞ | fully developed value |

## INTRODUCTION

Solid desiccant cooling and dehumidification systems have received considerable attention in the past several years as alternatives or supplements to conventional vapor compression machines for air conditioning buildings and spaces that have high latent loads. A desiccant cooling system involves passing humid (and warm) air through desiccant material for drying and a cooler (evaporative or refrigerative) for cooling to provide conditioned air. The desiccant becomes saturated with water and needs to be regenerated with hot air provided by an energy source. For buildings, the energy source can be the sun, natural gas, or off-peak electricity[1].*

A desiccant cooling system generally consists of an adiabatic desiccant dehumidifier, a heater, a regenerative heat exchanger, and two evaporative coolers. Efficient and compact components having a low pressure drop should be used in desiccant systems so that they can compete with vapor compression systems on energy savings, size, and cost. The heart of any desiccant system is the desiccant dehumidifier. The performance of a dehumidifier depends on its geometry and the type of desiccant used. Silica gel, a porous

---

*The superscript numbers are reference numbers.

material, is usually recommended as the solid desiccant for low-temperature regeneration applications[1] because of its high moisture recycling capacity and other desirable properties. Laminar-flow channel geometries (e.g., parallel plate) have been recommended as those with high heat and mass transfer performances and low pressure drops[2].

In a dehumidifier, heat and mass is transferred between air and the porous desiccant simultaneously. We must obtain the heat and mass transfer and pressure drop characteristics of a dehumidifier to evaluate its potential for use in desiccant cooling systems. We have used adiabatic heat and mass transient tests of dehumidifiers to provide such characterizations[3,4].

This paper presents the results of experimental and theoretical efforts to investigate the simultaneous heat- and mass-transfer and pressure-drop characteristics of three laminar flow dehumidifier test matrices. These efforts also provided information as to which dehumidifier matrix performed more efficiently and would be suitable for desiccant cooling systems. This paper is based on the results of two comprehensive reports[5,6]. This work complements the previous study of Maclaine-cross and Pesaran[7].

## EXPERIMENTAL METHOD

### Test Articles

Initially we tested and analyzed two test articles (a crushed-silica-gel parallel-plate matrix and a microbead-silica-gel staggered-parallel-strip matrix)[5,7]. Because the material and geometry were changed simultaneously, some of the results were not conclusive. We then tested a microbead-silica-gel parallel-plate matrix so we could make a direct comparison[6].

All three test matrices were fabricated in the same manner. Both sides of a polyester tape were coated with fine particles of silica gel. The coated tape (or sheet) with spacers attached to both sides were stacked in a supporting metal frame and stretched from both ends to make uniform channels. This gave the channel walls a fine coating of desiccant particles. Fig. 1 shows the schematic of the parallel-plate geometry and Fig. 2 shows the schematic of the staggered-parallel-strip geometry.

Crushed and microbead silica gels are both microporous and have practically the same thermophysical properties. The difference is that the crushed silica gel has larger particles ($d_p \approx 177$-297 μm) and irregular shapes and the microbead silica gel has smaller particles ($d_p \approx 74$-105 μm) with a more uniform, spherical shape. Table 1 compares the major specifications of the three test dehumidifier matrices.

### The Experimental Apparatus

The experimental apparatus was fabricated to obtain adiabatic step transient adsorption, desorption, and pressure drop data of a prototypical section of a desiccant dehumidifier. Fig. 3 shows a schematic of the experimental apparatus. The apparatus consists of a duct heater, a humidifier, a variable speed blower, an orifice plate, a test section, and instrumentation (hardware and software) for controlling and measuring temperatures, pressure drops, humidities, and airflow rates. The test section (which contains a test article, temperature sensors, air samplers for humidity measurement, and pressure taps) has a rectangular cross section of 0.161 m × 0.173 m and is 0.6 m long. The test section is insulated for adiabatic operation. Three butterfly valves are used to send air through the test section or through a bypass.

Important quantities to measure in these experiments are inlet and outlet temperatures and humidities,
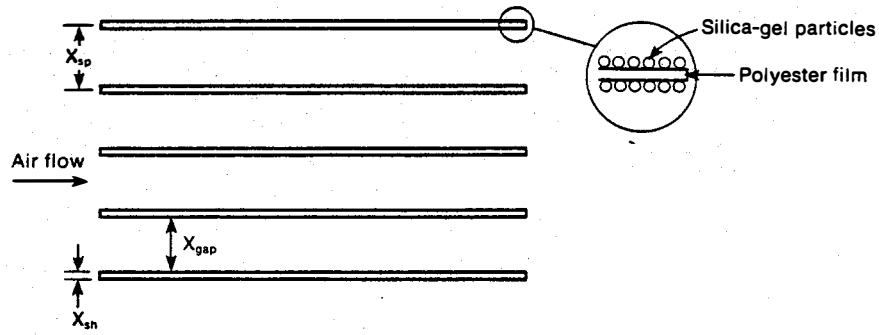
FIG. 1 PARALLEL-PLATE GEOMETRY
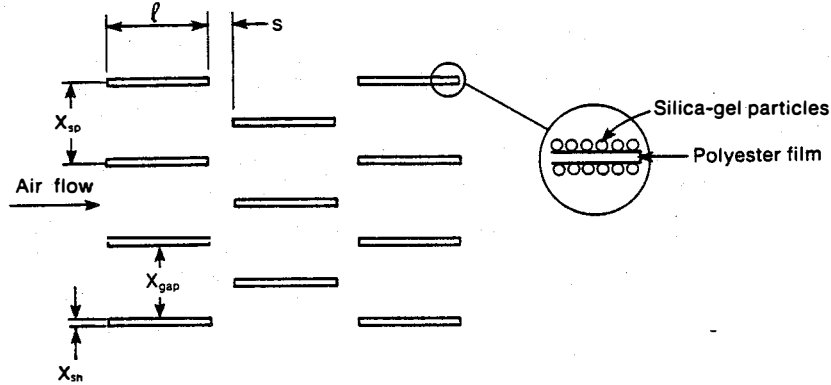


FIG. 2 STAGGERED PARALLEL-STRIP GEOMETRY
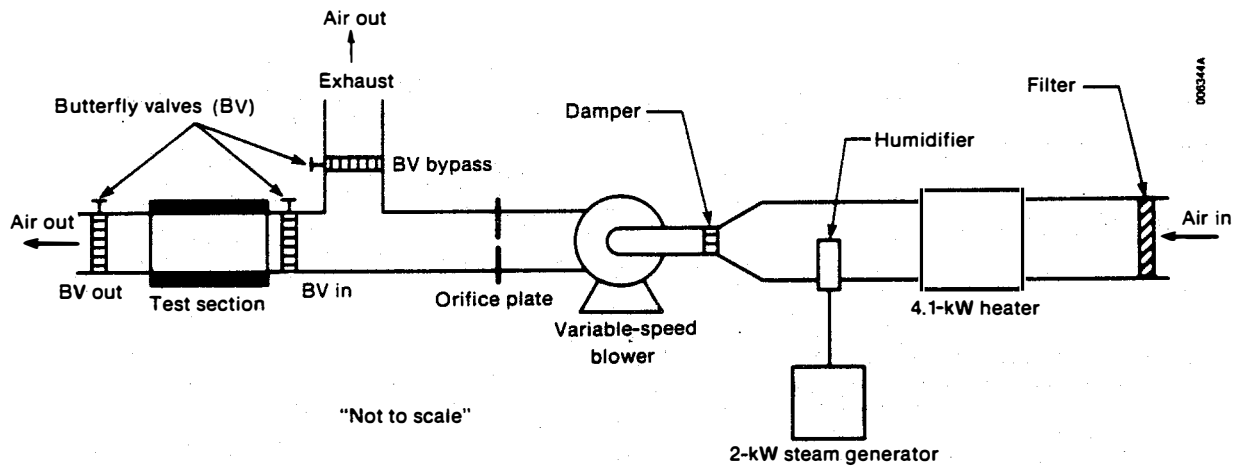


FIG. 3 EXPERIMENTAL APPARATUS

mass flow rate of air, and pressure drop across the dehumidifier. The temperature and humidity of air going through the bypass are also measured before introducing the air to the test article. A data acquisition system, consisting of personal computers and a voltmeter/scanner/multiplexer, collects the data and also controls the air humidity and temperature.

Air temperatures are measured using copper-constantan thermocouple wires. The uncertainty in temperature measurement is estimated to be less than 0.3°C. Air humidities are measured using optical condensation dew-point hygrometers with an uncertainty of less than 3% in humidity ratios. The pressure drop across orifice plates and test dehumidifiers are

3

**Table 1. Comparison of Specifications of Dehumidifier Test Matrices**

| Test Article | Crushed Silica Gel Parallel Plate | Microbead Silica Gel Parallel Plate | Microbead Silica Gel Staggered |
|---|---|---|---|
| Desiccant | Crushed silica gel | Microbead silica gel | Microbead silica gel |
| Geometry | Parallel plate | Parallel plate | Staggered parallel strip |
| Particle Size $d_p$ (μm) | 177-297 | 74-105 | 74-105 |
| Avgerage Particle Size (μm) | 237 | 89.5 | 89.5 |
| Polyester Film Thickness (μm) | 76 | 30 | 30 |
| Avgerage Sheet Thickness $X_{sh}$ (μm) | 550 | 209 | 209 |
| Dimensions (m) (W×H×L) | 0.117×0.126×0.203 | 0.116×0.125×0.199 | 0.115×.125×.196 |
| Estimated Average Air Gap × $X_{gap}$ (μm) | 1114 | 1101 | 1145 |
| Minimum Hydraulic Diameter (μm) | 1988* | 2140* | 2299* |
| Strip Length, $\ell$ (μm) | - | - | 6350 |
| Streamwise Spacing between Strips, s (μm) | - | - | 2000 |
| Surface Area/Volume ($m^2/m^3$) | 1202 | 1526 | 1147 |
| Mass of Desiccant (kg) | 0.497 | 0.188 | 0.137 |

*$d_h = 4 A_c L/A$

measured using capacitance-type pressure transducers with an uncertainty of less than 1.0%. Air mass flow rates are determined by ISO-standard orifice plates with an uncertainty of less than 3%.

**Experimental Procedure**

A test article is installed in the test section of the apparatus to obtain its adiabatic step transient response. Adiabatic step transient tests consist of obtaining the transient combined heat- and mass-transfer response of a dehumidifier matrix after a step change in the inlet air temperature, humidity or both. The inlet and outlet air temperatures and humidity ratios are measured as a function of time until the matrix reaches equilibrium with the inlet air. The matrix is initially at equilibrium with the air that has a different state than the inlet air state before the step change.

Each step transient test basically consists of three parts: matrix conditioning, process air preparation, and transient response. First, the dehumidifier matrix is conditioned for a uniform state (temperature and desiccant water content) by passing air of a desired condition through it until equilibrium is reached. The matrix is then sealed and isolated from the rest of the system. Second, the process airstream is brought up to a new state while it passes through a bypass section. Finally, when the process airstream reaches the desired humidity, temperature, and flow

rate, it is abruptly introduced to the matrix and the transient response is obtained. If the initial state of the matrix is drier than that of the process air, the test is called adsorption or dehumidification. A desorption or regeneration test occurs when the process air is drier than the initial state of the matrix. The pressure drop across the test dehumidifier as a function of mass air flow rate is also recorded for pressure drop characterization of the test matrix.

**METHOD OF ANALYSIS**

**Heat and Mass Transfer**

The common method for analyzing the adiabatic transient response of a dehumidifier test matrix has been a graphical one[3,4]: graphs of measured outlet temperature and humidity as a function of time were compared with the results of numerical finite difference models or approximate analytical solutions to extract the unknown parameters such as heat and mass transfer coefficients. At times, it has been difficult to make the curves match over a range of parameters relevant to the operation of dehumidifiers. This is because the predicted curves were sensitive to various unknown parameters. Because of method's limitations, we developed a new     for estimating dehumidifier matrix properties, such as effective desiccant mass and heat and mass transfer coefficients. In this method, we use all the experimental

4

data points for extracting the unknowns rather than the judgmental curve-matching technique. This technique combines the moments method and heat and mass transfer analogy theory. A brief description of this method[5] is given here.

In the heat and mass transfer analogy theory, the coupled heat and mass transport and conservation differential equations describing the behavior of a desiccant dehumidifier are transformed into sets of uncoupled differential equations describing the performance of two ($F_1$ and $F_2$) combined potentials[8]. The combined potentials $F_1$ and $F_2$ (which are similar to enthalpy and moisture content) depend on temperature, humidity, and the properties of air/water-vapor/desiccant. The combined potentials can then be treated like a heat-transfer-alone problem. The transient response (outlet temperature as a function of time) of a nondesiccant matrix (i.e., heat transfer alone) can be analyzed by the method of statistical moments[9] to calculate the heat transfer coefficient. It can be shown using Laplace transforms (e.g., Jefferson[10]) that the number of heat transfer units $N_{tu}$ for a constant specific heat system is related to normalized spread $\sigma/\mu$ by

$$N_{tu} = 2/(\sigma/\mu)^2 , \qquad (1)$$

where $\sigma/\mu$ is obtained from the moments method from

$$\left(\frac{\sigma}{\mu}\right)^2 = \frac{_0\int^\infty dT' \; _0\int^\infty \theta'^2 \; dT'}{\left(_0\int^\infty \theta'^2 dT'\right)^2} - 1 . \qquad (2)$$

This moments method is similar to the "maximum slope" technique used by Locke[11] to obtain heat transfer characteristics of several porous solids, which has been reported in Kays and London's Compact Heat Exchangers. The Nusselt number may be calculated from the number of transfer units of flow, matrix dimensions, and fluid properties

$$Nu = Re \; Pr \; N_{tu} \; Ac/A . \qquad (3)$$

The advantage of this method is that all data points can be used. Electronic digital data loggers have a high reading rate, and using all the data allows digitizing, which minimizes the random errors.

In the combined technique of statistical moments method and analogy theory, the experiment heat and mass transfer responses are first converted to the $F_1$ and $F_2$ responses; then they are treated as a heat-transfer-alone problem by the method of moments to obtain the number of transfer units for each potential [Eq. (1) and (2)] and then to calculate the Nusselt number of each combined potential $Nu_1$ and $Nu_2$ [from Eq. (3)]. The heat and mass transfer analogy theory is used once again to obtain the effective Lewis number Le (ratio of overall mass transfer resistance to overall heat transfer resistance) and overall heat transfer Nusselt number $Nu_0$ from

$$Nu_i = Nu_0 \; \frac{1 - (\alpha_i/\alpha_j \; Le)}{1 - \alpha_i/\alpha_j} \qquad i = 1,2, \; j = 3-i . \qquad (4)$$

where

$$\alpha_i = -(\partial T/\partial W)_{F_i} .$$

Then, the overall mass transfer $Nu_{mo}$ can be calculated from

$$Nu_{mo} = Nu_0/Le . \qquad (5)$$

The effective Lewis number is related through other properties of the matrix through the relation

$$Le = \frac{\alpha}{D_w} + Nu_0 \; \frac{\zeta_c}{\eta_a} , \qquad (6)$$

where the solid-side geometry factor coefficient $\zeta_c$ can be obtained from[12]

$$\zeta_c = \frac{1}{60 \rho_f} \left(\frac{d_p}{d_h}\right) \left(\frac{k}{\rho_d D_w}\right) \left(\frac{\partial w}{\partial W}\right)_T . \qquad (7)$$

The solid-side geometry factor $\eta_a$ is a correction factor to account for the desiccant particles that are not spherical and depends on the shape of the particles and how they cover the matrix geometrically. The factor, $\eta_a$, can be estimated from Eq. (4) and (6) if one knows the physical properties of air and the matrix and $Nu_1$ and $Nu_2$ from the analysis. The factor, $\eta_a$, should be a positive number and less than one. The overall mass-transfer resistance to moisture diffusion $S_o$ is the sum of the gas-side resistance $S_g$ and the solid-side resistance $S_s$; i.e.,

$$S_o = S_g + S_s . \qquad (8)$$

The gas-side resistance can be obtained from

$$S_g = \frac{1}{h_{mg}} , \qquad (9)$$

where the gas-side mass-transfer coefficient $h_{mg}$ can be calculated from

$$h_{mg} = \frac{Nu_m \; \rho \; D_w}{d_h} . \qquad (10)$$

Using the definition of the effective Lewis number, we can obtain

$$S_s = S_g \big( Le/(\alpha/D_w) - 1 \big) . \qquad (11)$$

Note that the effective Lewis number of 1 does not imply a zero solid-side diffusion resistance. When there is no solid-side resistance, the moisture diffusion in the solid is as fast as moisture diffusion in the air, and the effective Lewis number is $\alpha/D_w$.

The active mass of dry desiccant $m_d$ in the matrix is estimated from the moisture transferred between the process air and the desiccant and the equilibrium isotherms of the desiccant:

$$m_d = \frac{\int_{\theta_s}^{\theta_e} (W_i - W_o) \dot{m}_a \; d\theta}{W_e - W_s} . \qquad (12)$$

where $(W_e - W_s)$ is the difference between the moisture content of the matrix at the start and the end of the run.

## Pressure Drop

The measured pressure drop across a test matrix is slightly different than the actual pressure drop because the measuring pressure taps are about 50 mm upstream and downstream of the matrix. The actual, pressure drop across the matrix is

$$\Delta P_{actual} = \Delta P_{measured} - \Delta P_{inlet} - \Delta P_{outlet} . \qquad (13)$$

5

Inlet and outlet pressure drops were estimated using conservation of momentum and continuity. We can define the dimensionless pressure drop (according to Maclaine-cross and Ambrose[13]) by

$$(fRe)_{actual} = \frac{\Delta P_{actual}\, d_h^{'2}}{2\, \mu_m\, u_m\, L}\,, \quad (14)$$

where $d_h'$ is the hydraulic diameter for momentum transfer and can be different than the heat and mass transfer hydraulic diameter $d_h$.

The Reynolds number in the parallel passages of the parallel-plate test matrices is between 100 to 500 and the flow is expected to be laminar. Assuming fully developed laminar flow and uniform parallel-plate passages and constant properties for the parallel-plate matrices, we can write

$$fRe = \frac{\Delta P\, d_h^{'2}}{2\, \mu_m\, u_m\, L} = f_\infty\, Re_m + K_\infty\, \frac{Re_m\, d_h'}{4L}\,, \quad (15)$$

where $K_\infty = 0.686$ is the pressure drop coefficient for entrance effect inside a passage[13] and $f_\infty$ is the local Fanning friction factor for fully developed flow. For a rectangular passage $f_\infty$ is[14]

$$f_\infty = \frac{24}{Re}\, \frac{1}{(1 + X_{gap}/W)^2 (1 - 0.6329249\, X_{gap}/W)}\,, \quad (16)$$

where W is the width of the matrix.

The pressure loss across the staggered parallel-strip test matrix can be considered the summation of losses in passages plus the downstream losses. It can be shown[5] that

$$fRe = \frac{\Delta P\, d_h^{'2}}{2\, \mu_m u_m\, L} = f_\infty\, Re_m + K'\, \frac{Re_m\, d_h'}{\Delta L} \quad (17)$$

where

$$K' = K_\infty + \left[ K_\infty + 1 + \left(\frac{X_{gap}}{X_{gap} + X_{sh}}\right)^2 - \right.$$

$$\left. 2.4\left(\frac{X_{gap}}{X_{gap} + X_{sh}}\right)\right] \times L/\ell\,. \quad (18)$$

The terms $f_\infty$ and $K_\infty$ are the values for the parallel-plate duct given before.

To estimate dehumidifier matrix characteristics from the step transient tests using the methods outlined in this section, we developed a program called SINGLEBLOW[5] in Pascal that runs on an IBM or a compatible personal computer. The specifications of the test matrix, such as dimensions and desiccant properties, are entered in the program; the program is run with the experimental data and $Nu_1$ and $Nu_2$, and other pertinent values of the matrix are calculated.

## RESULTS AND DISCUSSION

We obtained adiabatic step transient data in the experimental apparatus for the microbead-silica-gel parallel-plate test matrix for this study and analyzed the data. We performed 32 experiments including redundant runs to verify experimental accuracy. Because of space limitations, we have summarized in Table 2 the conditions and results of analysis for only 12 of these experimental runs. Only two typical experiments (one adsorption and one desorption) are presented here in Figs. 4 and 5 in graphical forms. The results on the microbead-silica-gel parallel-plate matrix are compared here with the results previously obtained[7] on crushed-silica-gel parallel-plate and microbead-silica-gel staggered-parallel-strip test matrices.

### Heat and Mass Transfer Results

The adiabatic step transient data obtained for the microbead-silica-gel parallel-plate test matrix were analyzed with the combined moments method and analog theory using the SINGLEBLOW program. The results of interpreting the data: i.e., $Nu_1$, $Nu_2$, $R_d$, and fRe are also presented in Table 2. We found that for some experiments, unacceptable negative values for $Nu_1$ were estimated as we observed with the first two test matrices. These negative values were replaced with zero as shown in Table 2. The zero values were not used for further analysis. The reason for these negative estimates follow.

There are two heat and mass transfer waves associated with the two combined potentials $F_1$ and $F_2$ that pass through the desiccant matrix, which we record during a transient test. The outlet humidity profile of the first wave that comes out of the matrix is fast and for some experiments cannot be detected correctly because it overlaps with the responses of the humidity sensor; i.e., the time response of the first wave is similiar to the time constant of the sensor. The esti-

Table 2. Summary of Adiabatic Step Transient Tests on the Microbead Silica-Gel Parallel-Plate Matrix

| Run | Date (1986) | $P_t$ (Pa) | Matrix T (K) | Matrix w (g/kg) | Inlet T (K) | Inlet w (g/kg) | Intersection T (K) | Intersection w (g/kg) | Re | $\Delta P$ (Pa) | fRe | $R_d$ | $Nu_1$ | $Nu_2$ |
|---|---|---|---|---|---|---|---|---|---|---|---|---|---|---|
| 32 | 10/02 | 81344 | 300.3 | 13.1 | 333.1 | 15.1 | 309.9 | 19.5 | 208.9 | 72.0 | 21.40 | 0.77 | 8.43 | 14.98 |
| 33 | 10/05 | 82963 | 337.3 | 8.4 | 304.5 | 15.4 | 338.6 | 8.5 | 284.1 | 92.6 | 22.23 | 0.42 | 2.46 | 2.46 |
| 35 | 10/10 | 81955 | 301.3 | 13.5 | 315.8 | 15.1 | 306.5 | 17.2 | 305.2 | 103.3 | 23.23 | 0.93 | 7.33 | 5.15 |
| 36 | 10/10 | 81955 | 311.8 | 12.4 | 303.2 | 14.9 | 312.1 | 12.5 | 295.8 | 92.0 | 22.74 | 0.52 | 0.00* | 3.10 |
| 39 | 10/13 | 81941 | 302.5 | 13.2 | 353.7 | 14.6 | 326.3 | 19.9 | 390.8 | 176.5 | 24.59 | 0.78 | 0.00* | 2.64 |
| 40 | 10/13 | 81822 | 340.0 | 8.7 | 304.4 | 14.6 | 335.2 | 8.1 | 376.6 | 126.4 | 22.89 | 0.62 | 0.00* | 2.95 |
| 43 | 10/14 | 82485 | 304.2 | 14.5 | 315.6 | 15.0 | 306.6 | 16.8 | 205.1 | 64.1 | 21.68 | 0.86 | 22.94 | 6.08 |
| 44 | 10/14 | 82645 | 311.1 | 11.7 | 303.4 | 15.1 | 312.2 | 12.3 | 185.2 | 53.6 | 21.30 | 0.56 | 0.00* | 1.89 |
| 47 | 10/16 | 82751 | 303.0 | 13.6 | 307.5 | 10.3 | 301.5 | 12.8 | 300.2 | 93.7 | 22.84 | 0.95 | 13.24 | 2.45 |
| 48 | 10/16 | 82605 | 306.1 | 9.4 | 307.6 | 17.3 | 313.7 | 13.2 | 301.0 | 95.6 | 22.75 | 0.82 | 15.71 | 2.52 |
| 49 | 10/16 | 82539 | 306.3 | 16.0 | 307.7 | 10.1 | 301.9 | 13.4 | 398.5 | 135.0 | 24.66 | 0.97 | 26.11 | 4.16 |
| 50 | 10/16 | 82539 | 307.4 | 9.5 | 307.8 | 15.0 | 312.1 | 12.7 | 398.4 | 136.5 | 24.48 | 0.79 | 0.00* | 5.93 |

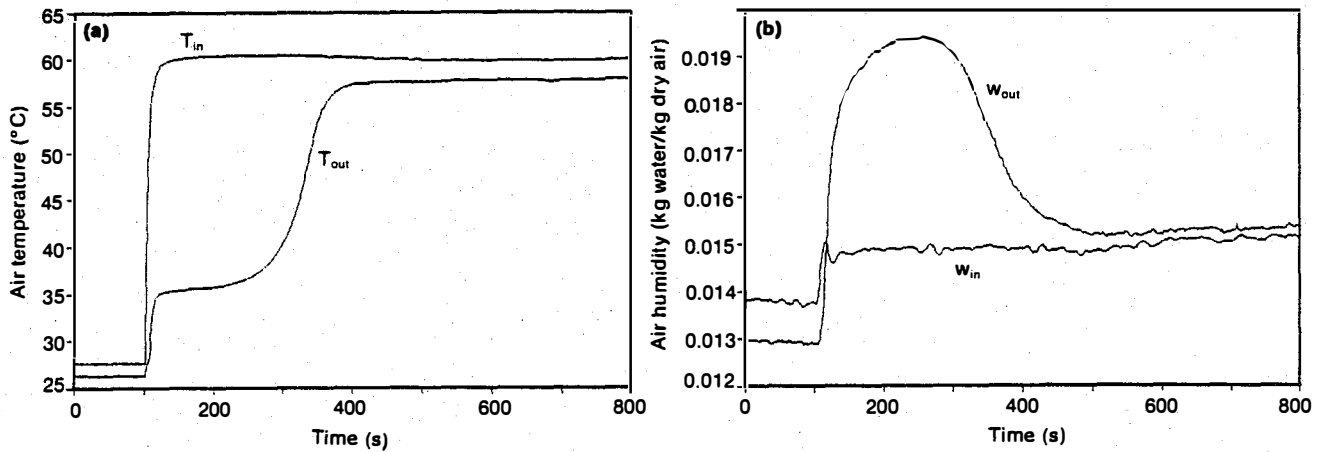*Negative values are replaced by zeros.

6

FIG. 4   TRANSIENT RESPONSE OF THE MICROBEAD SILICA-GEL/
PARALLEL-PLATE TEST MATRIX FOR A DESORPTION
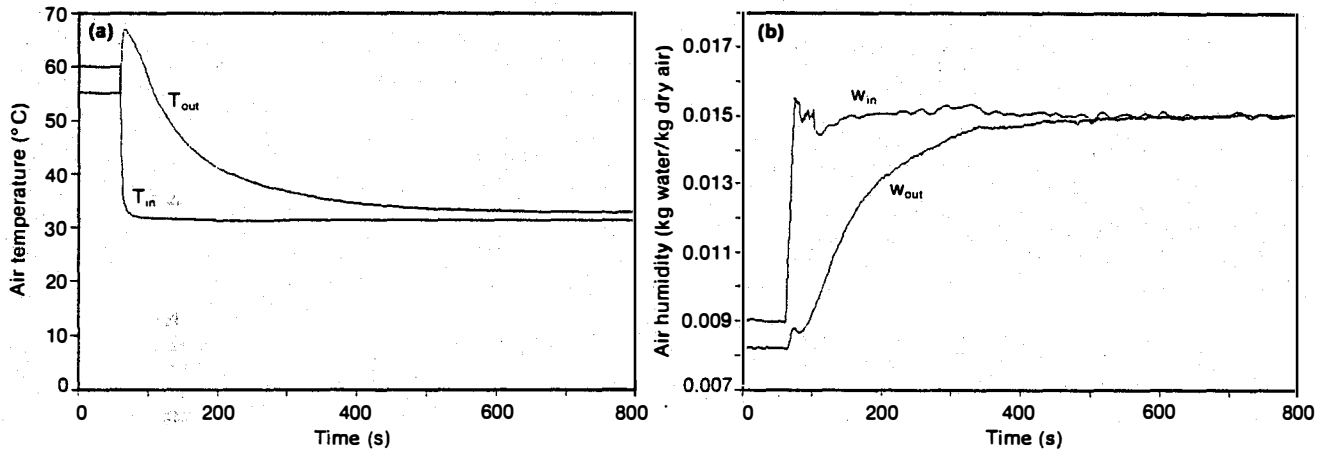EXPERIMENT (run 32)



FIG. 5   TRANSIENT RESPONSE OF THE MICROBEAD SILICA-GEL
PARALLEL-PLATE TEST MATRIX FOR AN ADSORPTION
EXPERIMENT (run 33)

mation of $Nu_1$ is sensitive to the profile of the first wave that passes through the matrix and can be in error. The values of $Nu_2$ are estimated independently of $Nu_1$ and are much more reliable. The mean value and mean relative error of $Nu_1$, $Nu_2$, and other pertinent values are estimated as shown in Table 3. Note that these means and relative errors are based on the results of all 32 experiments performed; the zero values were ignored in calculations of means; and the means of $Nu_1$ and $Nu_2$ were estimated based on the means of the normalized spreads $(\sigma/\mu)_1$, and $(\sigma/\mu)_2$.

Using these values of $Nu_i$ we estimated values of $\overline{Nu}_o$ and $\overline{Le}$ from Eq. (4) and $\eta_a$ from Eq. (6). Note that the required values of $\alpha_i/\alpha_j$, $\zeta_c$, and $\alpha/D_w$ for the calculations are outputs of the SINGLEBLOW program and their mean values and the associated errors are presented in Table 3. Unfortunately, using the estimated $Nu_1$ and $Nu_2$, we obtained values of Le smaller than $\alpha/D_w$ and negative values of $\eta_a$ that physically are not possible. Our calculations showed that this can be caused by using improper values of $Nu_1$. As mentioned before, an estimated $Nu_1$ can be wrong because the response of the dew-point hygrometer sensors interferes

with the first wave response of the test matrix. The values of $Nu_2$ and thus $Nu_2$ are more dependable than $Nu_1$, so we used the value of $\overline{Nu}_2$ and assumed a solid-side geometry factor $\eta_a = 1$, which is the maximum of $\eta_a$ and is also used by Bharathan et al.[15]. The factor $\eta_a = 1$ means that we have assumed the desiccant particles form a slab on the walls of the matrix.

Using Eq. (4) and (6) with $\eta_a = 1$, we found that for the microbead-silica-gel parallel-plate matrix, the mean overall heat transfer Nusselt number was 3.70 and the mean effective Lewis number was 1.0. The overall Nusselt number was about 50% lower than the convective number for the steady-state fully developed laminar flow in parallel-plate channels with constant heat flux boundary condition (Nu = 8.235). This is consistent with our previous observation for a crushed-silica-gel parallel-plate test matrix tested before[5,7]. The possibilities that can contribute to lowering the overall heat transfer Nusselt number from the convective heat transfer Nusselt number are:

o The presence of a stagnant air film between the particles and the main airstream in the passages that acts like a thermal resistance

7

**Table 3. Summary of Means and Errors of the Estimated Results for Microbead Silica-Gel Parallel-Plate Test Matrix**

| Parameter | Mean | Percent Error |
|---|---|---|
| $R_d$ | 0.79 | 6 |
| $Nu_1$ | 6.90* | 24* |
| $Nu_2$ | 3.71* | 15* |
| $fRe$ | 22.61 | 1 |
| $\alpha_1/\alpha_2$ | -2.11 | 13 |
| $\alpha/D_w$ | 0.86 | 0.2 |
| $\zeta_c$ | 0.038 | 9 |

*Calculated based on the mean of normalized spread.

o The effect of heat losses from the test article walls
o The effect of transient process
o The effect of mass transfer on heat transfer
o The effect of having nonuniform gaps in the matrix channels.

Under more ideal conditions, we can expect heat transfer Nusselt numbers, closer to the value of Nu = 8.235.

Table 4 compares the results of the transient tests on microbead-silica-gel parallel-plate geometries with the results of the tests performed on previous test articles: a parallel-plate matrix using crushed silica gel and a staggered parallel-strip matrix using microbead silica gel. Both parallel-plate test articles show similar average overall Nusselt numbers $\overline{Nu}_o$ that are much lower (about 80%) than that of the staggered-parallel-strip test article. The average effective Lewis number of all the test articles are close

(1.07 ±7%). The major difference between these test articles are desiccant particle size and geometry. From comparing the two parallel-plate test matrices, we observe that the mean $Nu_o$ is about the same, also the mean Le for the microbead-silica-gel parallel-plate matrix is less than the mean Le for the crushed-silica-gel parallel-plate matrix, which has larger crushed particles. This means that the resistance to moisture diffusion in the larger particles is more than the diffusion in the smaller particles, which is consistent with our expectations from Eq. (6) and (7). To estimate the dependence of the solid-side, moisture diffusion resistance $S_s$ in the particles of each test matrix, we used the analysis given for Eq. (8) through (11).

Table 5 shows the results of estimating mass transfer resistances in the three test articles based on the mean values estimated for the matrices. The solid-side resistances in the particles of the two matrices that have microbead particles are about the same (2.4 ±0.23 $sm^2/kg$) and are about 45% less than those of crushed particles of the parallel plate matrix. This is because the average size of the microbead-silica-gel particles is smaller (about one third that of crushed-silica-gel particles).

From the comparison between the two microbead test matrices, we can observe that the moisture diffusion resistances in their particles are about the same (Table 5), and the mean $Nu_o$ of the microbead-silica-gel staggered matrix is about 80% larger than the microbead-silica-gel parallel-plate matrix. This improvement was achieved as a result of a change in geometry (due to convective boundary layer breakup) as we expected. This boundary layer breakup also increases the pressure drop, as evidenced by an increase in $fRe$ of the staggered test article over the other two articles as shown in Table 4.

**Table 4. Summary of Momentum, Heat, and Mass Transfer Results of Three Test Matrices based on $\eta_a$ = 1**

| Dehumidifier Matrix | $\overline{Nu}_2$ | $\overline{Nu}_o$ | $\overline{Le}$ | $\overline{d}_p$ $(\mu m)$ | $\overline{fRe}$ | $\overline{Nu}_o/\overline{fRe}$ |
|---|---|---|---|---|---|---|
| Microbead Silica Gel Parallel Plate | 3.71 | 3.70 | 1.00 | 89.5 | 22.61 | 0.164 |
| Crushed Silica Gel Parallel Plate* | 3.48 | 3.59 | 1.14 | 23.7 | 25.48 | 0.141 |
| Microbead Silica Gel Staggered Parallel Strip | 6.57 | 6.68 | 1.06 | 89.5 | 36.87 | 0.181 |

*From Reference 5.

**Table 5. Estimated Mean Mass Transfer Resistances in the Test Matrices**

| Matrix | $\overline{d}_p$ $(\mu m)$ | Resistances Gas-side $S_g$ $(sm^2/kg)$ | Resistances Solid-side $S_s$ $(sm^2/kg)$ | Resistances Overall $S_o$ $(sm^2/kg)$ | $\overline{Nu}_{mo}$ |
|---|---|---|---|---|---|
| Crushed Silica Gel Parallel Plate | 237 | 14.53 | 4.77 | 19.30 | 3.15 |
| Microbead Silica Gel Staggered Parallel Strip | 89.5 | 8.99 | 2.20 | 11.19 | 6.30 |
| Microbead Silica Gel Parallel Plate | 89.5 | 15.56 | 2.64 | 18.20 | 3.70 |

The important parameters for comparing the three test articles are the ratio $Nu_o/fRe$ and $Le$. The ratio $Nu_o/fRe$ is a measure of rate of heat transfer to pressure drop and is one measure of dehumidifier efficiency and size. The effective Lewis number is a measure of resistance to the moisture diffusion in the particles and decreases with particle size as can be seen from Table 4.

A dehumidifier performs better or can be more compact with higher values of $Nu_o/fRe$ and lower values of $Le$[5]. Therefore, a dehumidifier using the smaller microbead-silica-gel particles and staggered parallel strip geometry can perform more efficiently (or be more compact) compared with the other two dehumidifiers previously discussed. This could reduce the size and cost of desiccant cooling systems. For further improvements in cost and performance, the focus should be on material choices and fabrication techniques.

## Pressure Drop Results

In addition to measuring pressure drop across the test matrix during each transient test, we also measured the pressure drop at various air flow rates at the end of two tests. At the end of these tests, the matrix was in equilibrium with the process airstream, which means that the heat and mass transfer processes were completed and thus there was minimal variation in air properties during these tests. The measured pressure drop across the test matrix is first corrected for inlet and outlet pressure drop [Eq. (13)]. Then it is made dimensionless using Eq. (14) and plotted as a function of dimensionless flow rate. The theoretical dimensionless pressure drop (fRe) across the test matrix is calculated using Eq. (15) and (17) for parallel-plate and staggered-parallel-strip matrices, respectively.
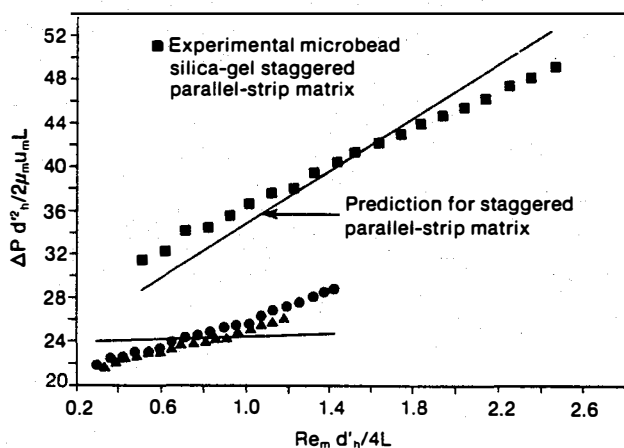
Fig. 6 shows the experimental and predicted pressure drop results for the three test matrices. The relative errors between the experimental and predicted values of fRe are -7% to +17% for the crushed-silica-gel parallel-plate matrix, -9% to +6% for the microbead-silica-gel parallel-plate matrix, and -7 to +9% for the microbead-silica-gel staggered-parallel-strip matrix. The magnitude of the errors may be explained by uncertainty in measurements of pressure drop, mass flow rate to a lesser extent, and the physical dimensions of the test articles (especially air gap sizes)

to a greater extent. However, the difference between the slopes K of the experimental and predicted curves cannot be explained by such errors. One possible explanation is that the predicted curves are based on the assumption that all the air passages of the matrix are uniform. If the gap sizes are not uniform, then the value of slope K will increase[15]. We are investigating the problem of nonuniformity to resolve the differences between experimental and predicted slopes.

## CONCLUDING REMARKS

We obtained adiabatic transient heat- and mass-transfer data and also pressure drop data for a microbead-silica-gel parallel-plate test dehumidifier. We analyzed the data and compared them with the results obtained previously on crushed-silica-gel parallel-plate and microbead-silica-gel staggered-parallel-strip test dehumidifiers and we concluded the following.

o The estimated average overall heat transfer Nusselt number for the microbead-silica-gel parallel-plate matrix was 3.70, which was slightly higher than that of crushed-silica-gel parallel-plate matrix (3.59) and lower than that of the microbead-silica-gel staggered-parallel-strip matrix (6.68). All these Nusselt numbers were about 40% to 55% lower than the convective Nusselt numbers predicted by steady-state laminar-flow theories for uniform passages. We postulated that these differences were caused by a combination of the following effects: nonuniformity in the gap size of the passages; the resistance in the stagnant air film between the main airstream in the passages and the different-size particles; heat losses from the walls; and transient simultaneous heat and mass transfer. Further investigation of these are required.

o By comparing the two microbead-silica-gel test matrices, we found that the overall heat- and mass-transfer Nusselt numbers of the staggered matrix were about 70% to 80% higher than those in the parallel-plate matrix. We also found that the solid-side resistance to the moisture diffusion in microbead particles of the two test matrices was about the same. This indicates that the estimation of the solid-side resistance is dependable. The increase in the overall transfer Nusselt numbers of the staggered matrix were because of an increase in the gas-side transfer Nusselt number caused by boundary layer breakups in the staggered geometry.



(a)
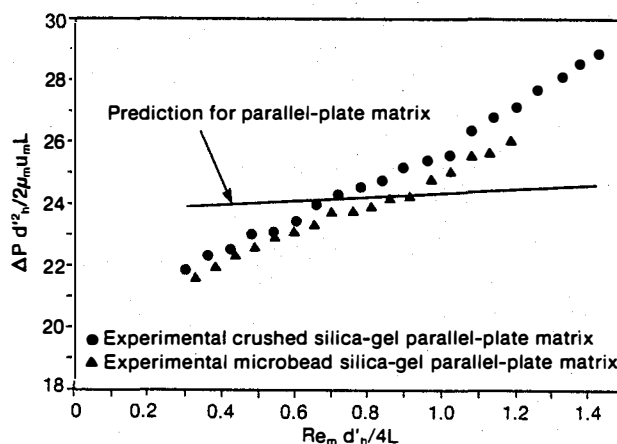
(b) Enlarged view of lefthand corner of (a)

FIG. 6 COMPARISON OF EXPERIMENTAL AND PREDICTED DIMENSIONLESS PRESSURE DROP FOR THE THREE TEST MATRICES

o By comparing the two parallel-plate test matrices, we found that the overall heat-transfer Nusselt numbers of the two matrices were about the same, while the overall mass transfer Nusselt number of the crushed-silica-gel matrix was 17% lower than the microbead-silica-gel matrix. This was caused by a greater solid-side moisture diffusion resistance resulting from the larger crushed-silica-gel particles. The solid-side resistance in the smaller microbead silica gel (average particle size = 89.5 μm) was about 45% less than that in the larger crushed silica gel (average particle size = 237 μm).

o The mean overall mass-transfer Nusselt number of the staggered-strip matrix was 100% higher than the crushed-silica-gel parallel-plate matrix because the 80% enhancement in gas-side transfer process and the 20% enhancement in solid-side transfer process.

o Although the experimental pressure drops across the dehumidifiers were of the same magnitude as the theory predictions, the slopes of the experimental curves were different than the slopes of the predicted curves. This difference could be explained if the test articles had nonuniform gap sizes. We are investigating the reason for the difference in trends of theoretical and experimental pressure drop curves.

o The ratio of heat or mass transfer to pressure drop $(Nu/fRe)$ of the microbead-silica-gel staggered-parallel-strip matrix was about 28% higher than that of the crushed-silica-gel parallel-plate matrix and 10% higher than that of the microbead-silica-gel parallel-plate matrix. Fabricating a dehumidifier with a staggered-parallel-strip geometry and microbead silica gel will result in a smaller and probably less expensive dehumidifier than one using crushed or microbead silica gel with a parallel-plate geometry.

## ACKNOWLEDGMENTS

## REFERENCES

1. Jurinak, J. J., "Open Cycle Desiccant Cooling--Component Models and Systems Simulations," Ph.D. Dissertation, Madison, WI: University of Wisconsin, Solar Energy Laboratory, 1982.

2. Schlepp, D., and K. Schultz, "Analysis of Advanced Solar Hybrid Desiccant Cooling Systems for Buildings," SERI/TR-252-2527, Golden, CO: Solar Energy Research Institute, 1984.

3. Kim, S., P. Biswas, and A. F. Mills, "A Compact Low-Pressure Drop Desiccant Bed for Solar Air-Conditioning Application, 2: Bench Scale Tests, J. Solar Energy Eng., Vol. 107, 1985, pp. 120-127.

4. Bullock, C. E., and J. L. Threlkeld, "Dehumidification of Moist Air by Adiabatic Adsorption," Trans. Am. Soc. Heat Refrig. Air-Condit. Eng., Vol. 72, 1966, pp. 301-313.

5. Pesaran, A. A., I. L. Maclaine-cross, and E. Van den Bulck, Measurements on Promising Dehumidifier Materials and Geometries, SERI/TR-252-2898, Golden, CO: Solar Energy Research Institute, forthcoming.

6. Pesaran, A. A., J. Parson, and K. Dukehart, Experiments on Desiccant Materials and Geometries for Desiccant Dehumidifiers, SERI/TR-252-3065, Golden, CO: Solar Energy Research Institute, forthcoming.

7. Maclaine-cross, I. L., and A. A. Pesaran, "Heat and Mass Transfer Analysis of Dehumidifiers using Adiabatic Transient Tests," presented at the AIAA/ASME 4th Thermophysics and Heat Transfer Conference, June 1986, Boston, MA.

8. Banks, P. J., D. J. Close, and I. L. Maclaine-cross, "Coupled Heat and Mass Transfer in Fluid Flow through Porous Media--An Analogy with Heat Transfer," Proc. 4th Int. Heat Transfer Conf., Versailles, 1970.

9. Ruthven, D. M., Principles of Adsorption and Adsorption Processes, New York: John Wiley & Sons, Inc., 1984.

10. Jefferson, C. P., "Dynamic of Packed Beds with Intraphase Heat and Mass Transfer," Chemical Engineering Science, Vol. 23, 1968, pp. 509-523.

11. Locke, G. L., "Heat Transfer and Flow Friction Characteristics of Porous Solids," Technical Report No. 10, Department of Mechanical Engineering, Stanford University, Stanford, 1950.

12. Maclaine-cross, I. L., "A Theory of Combined Heat and Mass Transfer in Regenerators," Ph.D. Dissertation, Australia: Monash University, Department of Mechanical Engineering, 1974.

13. Maclaine-cross, I. L., and C. W. Ambrose, "Predicted and Measured Pressure Drop in Parallel-Plate Rotary Regenerators," ASME Journal of Fluids Engineering, Vol. 102, Mar. 1980, pp. 59-63.

14. Cornish, R. J., "Flow in a Pipe of Rectangular Cross-Section," Proceedings of the Royal Society, Sec. A, Vol. 120, 1928, pp. 691-700.

15. Bharathan, D., I. L. Maclaine-cross, and J. R. Parsons, Experimental Studies of Heat and Mass Exchange in Parallel-Passage Rotary Desiccant Dehumidifiers for Solar Cooling Applications, SERI/TR-252-2897, Golden, CO: Solar Energy Research Institute, forthcoming.